Ultrafast Surface State Spin-Carrier Dynamics in the Topological Insulator Bi_2Te_2Se

Vasudevan Iyer,[1] Yong P. Chen,[2] and Xianfan Xu[1,*]
[1]Department of Mechanical Engineering and Birck Nanotechnology Center, Purdue University, West Lafayette, Indiana 47907, USA
[2]Department of Physics and Astronomy and School of Electrical and Computer Engineering and Birck Nanotechnology Center and Purdue Quantum Center, Purdue University, West Lafayette, Indiana 47907, USA

(Received 14 March 2018; revised manuscript received 6 May 2018; published 11 July 2018)

Topological insulators are promising candidates for optically driven spintronic devices, because photoexcitation of spin polarized surface states is governed by angular momentum selection rules. We carry out femtosecond midinfrared spectroscopy on thin films of the topological insulator Bi_2Te_2Se, which has a higher surface state conductivity compared to conventionally studied Bi_2Se_3 and Bi_2Te_3. Both charge and spin dynamics are probed utilizing circularly polarized light. With a sub-band-gap excitation, clear helicity-dependent dynamics is observed only in thin (<20 nm) flakes. On the other hand, such dependence is observed for both thin and thick flakes with above-band-gap excitation. The helicity dependence is attributed to asymmetric excitation of the Dirac-like surface states. The observed long-lasting asymmetry over 10 ps even at room temperature indicates low backscattering of surface state carriers which can be exploited for spintronic devices.

DOI: 10.1103/PhysRevLett.121.026807

Topological insulator (TI) surface states possess properties such as spin-momentum locking and backscattering protection [1–5] and high mobility [6–8] which make them suited for spintronics applications [9,10]. A long spin lifetime ensures that information carried by spin is not lost during device operation [11,12]. Therefore, surface states (SS) protected from backscattering are natural candidates for the task. Furthermore, their high mobility can afford faster switching of devices. The widely studied Dirac states in graphene exhibit long spin diffusion lengths upon electrical injection of spin [13,14]. However, they lack spin-momentum locking, which prevents branch selective optical injection of spin. On the other hand, circularly polarized light has been shown theoretically [15] and experimentally [16,17] to excite only one branch of the spin-momentum locked surface states in TIs. Optical spin control is thus an alternative to conventional magnetic or electric control of devices [18,19]. It is therefore important to examine the interaction of light with SS and understand the resulting charge carrier and spin dynamics.

The fundamental carrier relaxation dynamics of the Dirac-like SS following photoexcitation has been studied using angle-resolved photoemission spectroscopy (ARPES) [20–28], terahertz pump-probe spectroscopy [29,30], photoluminescence spectroscopy [31], and optical pump-probe spectroscopy [32–34]. ARPES utilizes energy windows to independently track relaxation of the conduction band, valence band, SS, and the coupling between bulk and SS. Most studies used an above-band-gap pump and probe energy with linear polarization resulting in interband transitions along with uniform excitation of both branches of the Dirac cone. There is, however, very limited literature on using circularly polarized light to create asymmetric excitations in the SS and study spin dynamics, which is more relevant to optical spin control. Most of the aforementioned works focused only on charge dynamics. Wang and co-workers studied the spin dynamics in Bi_2Se_3 of the second Dirac cone lying above the bulk conduction band and found subpicosecond relaxation [35]. Similarly, Hsieh *et al.* observed a subpicosecond spin relaxation in Bi_2Se_3 using second harmonic probing [34]. Recently, Kuroda and co-workers demonstrated asymmetric excitation of SS in Sb_2Te_3 lasting a few picoseconds with an excitation energy below the band gap [25,26]. Apart from the all-optical studies, an optoelectronic approach demonstrated a spin lifetime of several picoseconds in Bi_2Se_3 [36].

Compared to widely studied Bi_2Se_3 and Bi_2Te_3, topological insulators Bi_2Te_2Se (BTS) and $BiSbTeSe_2$ have better bulk insulating properties due to the Fermi level being situated near the middle of the band gap [37,38]. Hence, we chose BTS for our study and performed all-optical pump and probe measurements to investigate the timescales of charge and spin relaxation. We used an obliquely incident, circularly polarized midinfrared or optical pump (7 μm, 0.17 eV and 800 nm, 1.55 eV) to excite both below and above the band gap (0.3 eV [39]). The probe was fixed at 7 μm. This avoids probing of interband transitions and allows exclusive study of the photon helicity-dependent dynamics of SS.

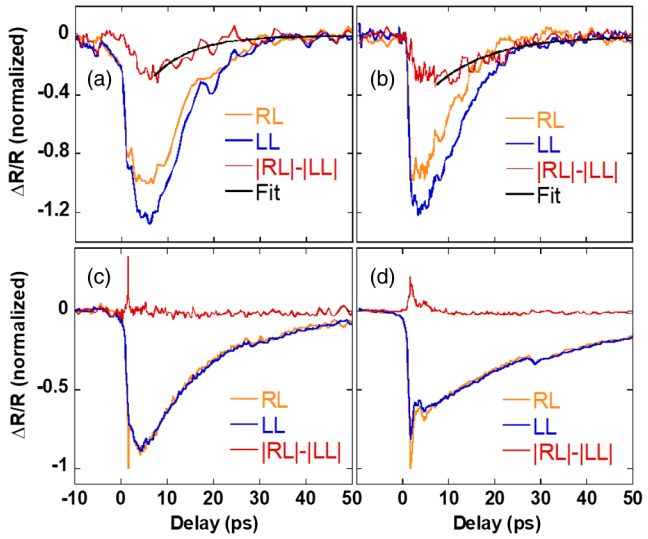

FIG. 1. Helicity-dependent dynamics for a (a) 14, (b) 18, (c) 45, (d) 75 nm flake with a 7 μm pump and a 7 μm probe. The difference, i.e., |RL|-|LL| vs time, can be fit with an exponential decay time $\tau = 8.2$ ps for (a) and $\tau = 12$ ps for (b).

We first examine transient dynamics with both excitation and probing energies of 0.17 eV (7 μm). Flakes of BTS with thicknesses between 14 and 75 nm were exfoliated on CaF_2. The sample preparation and experimental setup are described in Supplemental Material [40], note 1. Figure 1 shows the helicity- and thickness-dependent dynamics at room temperature. ΔR is the change in reflectance of the probe after pump excitation, i.e., $\Delta R = R_{\text{pump}}$-$R$, where R_{pump} and R are the reflectance with and without pump, respectively. LL (left circular pump, left circular probe) corresponds to the pump and probe having angular momentum pointing in the same direction with respect to the sample surface, and RL (right circular pump, left circular probe) corresponds to their angular momentum in opposite directions. A clear difference between RL and LL lasting for more than 10 ps is observed for 14 and 18 nm samples [Figs. 1(a) and 1(b)]. When the pump and probe have the same helicity, we observe a larger signal amplitude—LL has a larger amplitude than RL. The same trend is observed when changing the helicity of the probe instead of the pump—RR shows a larger signal than RL (Supplemental Material [40], Fig. S1). $\Delta R/R$ of both RL and LL are normalized to $|\text{RL}|_{\text{max}}$. The difference between LL and RL is also plotted as |RL|-|LL|. Furthermore, an exponential fit ($e^{-t/\tau}$) can be used to describe the decay of the difference, starting from the point of maximum change. The extracted decay time [$\tau = 8.2$ ps and $\tau = 12$ ps in Figs. 1(a) and 1(b)] quantifies spin relaxation due to the branch-selective excitations, which will be discussed later. The measurement was also conducted at 80 K (Supplemental Material [40], Fig. S2), but only a slightly greater difference between the RL and LL signals was observed.

For thicker samples [Figs. 1(c) and 1(d)], only a short-lived difference between the reflectance signals RL and LL is observed around time zero. Its origin could be coherent coupling of the pump and probe during temporal overlap and hence is not related to SS dynamics. The small bump near 30 ps is due to multiple reflection by the neutral density filter.

The decay time of the reflectivity signal quantifies charge relaxation. The charge decay times for 14 and 18 nm flakes are similar to the values reported for SS relaxation in ARPES studies [20,21], indicating that the dynamics observed in the thin flakes is dominated by SS. Theoretically, it has been predicted that charge and spin relaxation times should be the same on the Dirac cone of TIs [42]. From the experimental data, we see that the time duration when LL and RL are different, which indicates the spin decay time, is the same as the total decay time of the reflectivity signal. Hence, the dynamics is completely dominated by SS in thin flakes. We also noticed that the decay dynamics of thin flakes are similar to that of graphene, which has a Dirac origin. In Supplemental Material [40], Fig. S3 shows similar charge decay times for the 14 nm flake and graphene, supporting a Dirac origin for the BTS flakes.

The slower charge decay as the flakes get thicker is related to atmospheric doping of the samples due to gas adsorption that raises the Fermi level [43–47], leading to allowed SS to bulk conduction band transitions and excitations of free carriers. The slow relaxation is thus due to the interband relaxation from the conduction band to the SS or valence band, requiring additional scattering mechanisms such as phonon coupling or defect-assisted recombination as observed by other researchers [33]. It is reported that bulk samples undergo short-term atmospheric doping [46,47], and hence those flakes were likely to have been doped shortly after exfoliation. For our samples, electrical and thermal transport measurements on thin BTS films (<20 nm) have shown a dominating contribution of SS to thermal and electrical conductivity at room temperature as compared to thicker flakes (> 20 nm) [48]. The carrier concentration vs thickness, along with the Hall measurement [40,41], are shown in Supplemental Material [40], Figs. S4–S6, where it can be seen that sub-20-nm flakes have an order of magnitude lower carrier concentration. The obtained carrier concentration of $\sim 5 \times 10^{12}$ cm^{-2} per surface is only half that obtained from the ARPES measurement on a thick flake when the Fermi level is located at the bottom of the conduction band [43], indicating that the Fermi level is closer to the charge neutral point. The detailed information on Hall measurements was provided in Ref. [48]. Se vacancy migration to the surface and subsequent gas adsorption has been reported as a mechanism for surface doping [49,50]. Thicker films have many quintuple layers behind their surface, allowing for vacancy migration and formation of 2D electron gas and subsequent band bending at the surface. Thin flakes, on the other hand, have fewer migrating sites

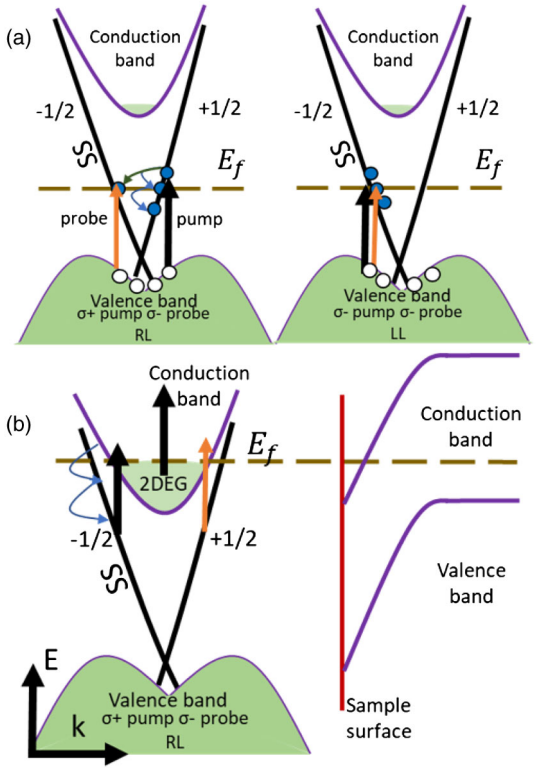

FIG. 2. Transition diagram with a 7 μm pump and a 7 μm probe for (a) thin samples with a relatively low Fermi level. The left figure illustrates the $\sigma+$ pump and $\sigma-$ probe (RL), and the right figure the $\sigma-$ pump and $\sigma-$ probe (LL). LL produces a stronger probe response than RL. (b) Thick samples with a high Fermi level for the $\sigma+$ pump and $\sigma-$ probe (RL), which does not produce a helicity-dependent signal (see the text). The black arrow represents the pump, and the orange arrow represents the probe.

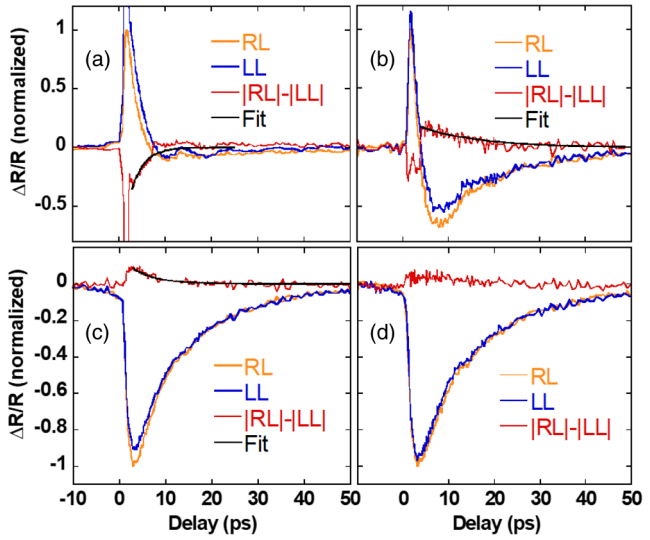

FIG. 3. Helicity dependence of a (a) 14, (b) 18, (c) 45, and (d) 75 nm sample with the 800 nm pump and the 7 μm probe. The difference |RL|-|LL| is fit with an exponential, $\tau = 2.8$ ps for (a), $\tau = 12.5$ ps for the positive part in (b), and $\tau = 5.3$ ps for (c). The fitting is poor for (d) and hence not shown.

due to the thinner bulk region and, hence, do not undergo as much of the surface doping.

We now proceed to explain the helicity-dependent dynamics using the band structure in Fig. 2(a), which depicts the Fermi level at 148 meV above the Dirac point as observed in an ARPES measurement for a freshly cleaved sample in a vacuum, not affected by atmospheric doping [43]. RL implies the $\sigma+$ pump and $\sigma-$ probe having angular momentum $+1$ and -1, respectively. We set the spin on the right side branch of SS $+1/2$ and on the left side $-1/2$. Hence, the in-plane component of a circularly polarized pump (black arrow) at an oblique incidence excites only the depicted transition due to conservation of in-plane angular momentum. Likewise, the circularly polarized probe (orange arrow) at an oblique incidence monitors only the depicted transition. The midinfrared pump pulses excite electrons from the valence band to the energy levels around the Fermi energy. In principal, a transition from SS to the conduction band is also possible. However, the large pool of valence electrons transitioning to SS competes with the SS to conduction band transition, making the latter contribute less. The probe, being of the same energy, monitors only SS. Therefore, when probing with the same helicity, the change in reflectance is expected to be larger because $\Delta R \sim \Delta f_1 * \Delta f_2$, where $f_1(k)$ and $f_2(k)$ are momentum-dependent Fermi occupation probabilities of the initial and final states. The holes generated in the valence band rapidly (<100 fs) redistribute in k space, making f_1 momentum independent, whereas the asymmetrically generated electrons in SS do not redistribute as fast due to the backscattering protection, making f_2 larger for the pumping side of the k space. Hence, the difference in the signals (RL-LL) gives the backscattering time, which is a net result of many small angle scattering events, and will be discussed in more detail later. The difference between the RL and LL in the thin flakes is about 20% of the signal amplitude, which is due to the out-of-plane component of the pump and probe that excites both branches of the Dirac cone simultaneously, giving rise to at least half of the total signal amplitude.

For thicker flakes, the Fermi level is raised as depicted in Fig. 2(b)[43]. The SS to conduction band excitation is now possible, which leads to interband relaxation and manifests as a slower decay in the signals. An important consideration is the hexagonal warping of the higher-energy surface states lying closer to the conduction band, resulting in out-of-plane spin components on an otherwise in-plane spin texture carried by the SS [51–54]. This could be one of the main reasons for the lack of clear helicity dependence in thick flakes owing to excitation of the higher-energy portion of the SS. The excitation of 2D gas electrons or defect states is another reason, as they do not have a helicity dependence.

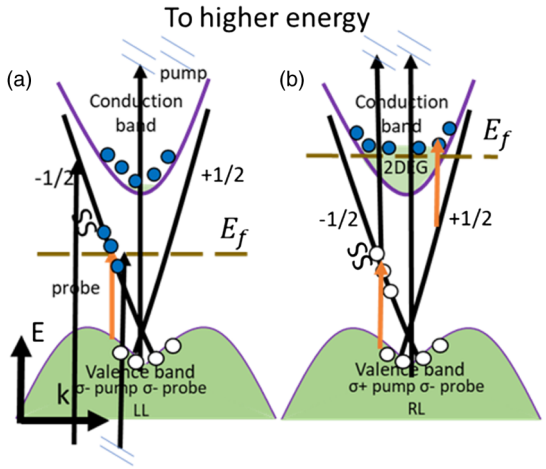

FIG. 4. Transition diagram for the 800 nm pump and the 7 μm probe for (a) thin samples with a low Fermi level for the $\sigma-$ pump and $\sigma-$ probe (LL), resulting in a stronger probe response for LL, and (b) thick samples with a high Fermi level, where RL has a stronger probe response (see the text). The black arrow is the pump, and the orange arrow is the probe.

We now examine above-band-gap excitation. Figure 3 shows that flakes of all thicknesses exhibit a helicity dependence but with a reducing magnitude of the difference (|RL|-|LL|) as the flakes become thicker. The difference can be once again fit with an exponential. For the 14 nm flake [Fig. 3(a)], the total signal decays rapidly, with a spin relaxation time (when RL and LL are different) of 2.8 ps, the same as the total signal decay time. The spin relaxation is hence limited by the charge relaxation itself, similar to what is observed with below-band-gap excitation [Fig. 1(a)]. It is known that excitation or probing close to the Fermi level shows a slower decay than excitations away from it due to the requirement of phonons for relaxation [55,56]. This is in good agreement with our observed timescales, since the 800 nm light can excite carriers much above the Fermi level within the Dirac state, whereas the 7 μm excites carriers in close proximity to the Fermi level. Here again LL has a larger signal than RL and can be explained using the transition diagram [Fig. 4(a)], where electrons are promoted to states near the Fermi level from deeper lying levels in the valence band. The sharp peak near time zero has been truncated for easier visualization.

Helicity dependence is also observed for the thicker flakes as shown in Figs. 3(c) and 3(d), which was absent with the 7 μm pump. This is because the 800 nm pump can excite almost all energy levels on SS, unlike the 7 μm pump, as illustrated in the transition diagram [Fig. 4(b)]. Moreover, RL has a larger signal amplitude, whereas in the 7 μm and 800 nm case for thin flakes LL has a larger amplitude. This can be explained based on Fig. 4(b). The allowed excitation for the 800 nm pump is reversed when the Fermi level is higher, because the initial state is now SS instead of the valence band. For example, a $\sigma+$ pump must excite electrons from the $-1/2$ branch of SS and result in $+1/2$ spin electrons in the conduction band [$\Delta = ½ - (-½) = 1$]. This means electrons from the left side $(-1/2)$ branch are preferentially depopulated by the right circular $(\sigma+)$ pump, but the left circular probe $(\sigma-)$ interrogates the left branch, thereby giving a larger signal magnitude. The obtained spin relaxation time is 5.3 ps for the 45 nm sample, but a spin relaxation time is not obtained for the 75 nm sample due to the very low differential signal. It is also not surprising to observe a charge decay time of close to 50 ps, which is similar to that for thick samples when pumped with 7 μm light. This leads to the conclusion that the bulk states continuously feed the surface states and relax via this channel as observed in the literature [20,33].

We now examine the data of the 18 nm flake [Fig. 3(b)]. We see that it shows features possessed by both 14 and 45/75 nm flakes, i.e., a negative and positive difference between RL and LL ($\tau = 12.5$ ps). This along with the diminishing difference [|RL|-|LL|, Figs. 3(a)–3(d)] with thickness is an indicator of an enhanced surface to bulk coupling as the flakes get thicker. A rapid flow of electrons and holes from the deeper layers towards the surface and subsequent relaxation through the Dirac states is a possible mechanism that reconciles the observation. That is, the influx of unpolarized carriers would diminish the signal difference, and at the same time those carriers would account for interband relaxation, which leads to slower relaxation. The 18 nm flake shows a similar spin-relaxation timescale with 7 μm and 800 nm excitation, because the expected faster relaxation (e.g., 14 nm flake) is offset by the bulk contribution in the latter case, prolonging the carrier lifetime. The influx of carriers could also explain the faster spin relaxation in the 45 nm flake (5.3 ps).

Another important aspect regarding the thickness-dependent spin and charge dynamics is small angle scattering of electrons due to phonons. SS electrons in 3D topological insulators are forbidden only from 180° backscattering in the k space but can undergo small angle scattering [3]. SS electrons in the very thin samples have little access to scattering with bulk phonons, resulting in reduced small angle scattering, and thus competing charge and spin relaxation is observed in our experiments [Figs. 1(a), 1(b), and 3(a)]. In contrast, thick samples can supply phonons and allow for faster decoherence of the SS electrons. This mechanism is in parallel to the influx of unpolarized carriers discussed previously.

Mean free paths for charge and spin diffusion in SS can be as long as 2 μm [57–59]. A few metals also have spin diffusion lengths of 100 nm or more [60]. With asymmetry lasting more than 10 ps and a Fermi velocity of 1×10^5 m/s [43], we estimate a spin diffusion length longer than 1 μm in our samples. This is in reasonable agreement with the aforementioned literature, especially for doping compensated materials. A perfectly tuned Fermi level in BTS shows

the SS population lasting as long as 6 μs [61,62]. Hence, BTS can be promising for spintronics. Also, spin relaxation times obtained in this work are comparable to valley depolarization times of a few picoseconds observed in valley nondegenerate transition metal dichalcogenides (TMDs) [63–65]. However, due to the massless nature of the Dirac-like fermions in TIs, we can expect them to perform comparable to or better than TMDs in spintronics.

In summary, we carried out oblique incidence, helicity-resolved optical pump-probe spectroscopy on topological insulator Bi_2Te_2Se using below- and above-band-gap excitation and showed that this technique is useful to study spin dynamics in topological insulators. With below-band-gap excitation, a clear helicity dependence was observed for flakes thinner than 20 nm. The vanishing helicity dependence in thick samples was attributed to the formation of 2D electron gas on the surface due to gas adsorption at vacancy sites. Above-band-gap excitation resulted in asymmetric excitation of surface states for both thin and thick samples. The polarization-resolved dynamics reveals the helical spin texture of the surface states and spin relaxation times in the 5–15 ps range, which translates to a micrometer spin diffusion length. Excitations with midinfrared circularly polarized light is therefore a possible route to control spintronic devices involving thin film topological insulators.

The authors thank Andres Llascahuanga for providing the graphene sample, Anurup Datta for help with AFM measurements, and Dr. Jifa Tian for the Hall measurements. We also thank Ireneusz Miotkowski for synthesizing the Bi_2Te_2Se crystals. Funding from the National Science Foundation (EFMA-1641101) is gratefully acknowledged.

The authors declare no competing financial interests.

*xxu@ecn.purdue.edu

[1] L. Fu and C. L. Kane, Phys. Rev. B **76**, 045302 (2007).
[2] Y. Xia, D. Qian, D. Hsieh, L. Wray, A. Pal, H. Lin, A. Bansil, D. Grauer, Y. S. Hor, R. J. Cava, and M. Z. Hasan, Nat. Phys. **5**, 398 (2009).
[3] P. Roushan, J. Seo, C. V. Parker, Y. S. Hor, D. Hsieh, D. Qian, A. Richardella, M. Z. Hasan, R. J. Cava, and A. Yazdani, Nature (London) **460**, 1106 (2009).
[4] T. Zhang, P. Cheng, X. Chen, J. F. Jia, X. C. Ma, K. He, L. L. Wang, H. J. Zhang, X. Dai, Z. Fang, X. C. Xie, and Q. K. Xue, Phys. Rev. Lett. **103**, 266803 (2009).
[5] J. F. Tian, I. Miotkowski, S. Hong, and Y. P. Chen, Sci. Rep. **5**, 14293 (2015).
[6] J. G. Checkelsky, Y. S. Hor, R. J. Cava, and N. P. Ong, Phys. Rev. Lett. **106**, 196801 (2011).
[7] N. Koirala, M. Brahlek, M. Salehi, L. Wu, J. X. Dai, J. Waugh, T. Nummy, M. G. Han, J. Moon, Y. M. Zhu, D. Dessau, W. D. Wu, N. P. Armitage, and S. Oh, Nano Lett. **15**, 8245 (2015).
[8] N. P. Butch, K. Kirshenbaum, P. Syers, A. B. Sushkov, G. S. Jenkins, H. D. Drew, and J. Paglione, Phys. Rev. B **81**, 241301 (2010).
[9] Y. Q. Huang, Y. X. Song, S. M. Wang, I. A. Buyanova, and W. M. Chen, Nat. Commun. **8**, 15401 (2017).
[10] A. A. Baker, A. I. Figueroa, L. J. Collins-McIntyre, G. van der Laan, and T. Hesjedal, Sci. Rep. **5**, 7907 (2015).
[11] P. Chuang, S.-C. Ho, L. W. Smith, F. Sfigakis, M. Pepper, C.-H. Chen, J.-C. Fan, J. P. Griffiths, I. Farrer, H. E. Beere, G. A. C. Jones, D. A. Ritchie, and T.-M. Chen, Nat. Nanotechnol. **10**, 35 (2015).
[12] Y. G. Semenov, K. W. Kim, and J. M. Zavada, Appl. Phys. Lett. **91**, 153105 (2007).
[13] C. C. Lin, A. V. Penumatcha, Y. F. Gao, V. Q. Diep, J. Appenzeller, and Z. H. Chen, Nano Lett. **13**, 5177 (2013).
[14] P. J. Zomer, M. H. D. Guimaraes, N. Tombros, and B. J. van Wees, Phys. Rev. B **86**, 161416(R) (2012).
[15] P. Hosur, Phys. Rev. B **83**, 035309 (2011).
[16] M. R. Scholz, J. Sanchez-Barriga, J. Braun, D. Marchenko, A. Varykhalov, M. Lindroos, Y. J. Wang, H. Lin, A. Bansil, J. Minar, H. Ebert, A. Volykhov, L. V. Yashina, and O. Rader, Phys. Rev. Lett. **110**, 216801 (2013).
[17] M. Xia, J. Jiang, Z. R. Ye, Y. H. Wang, Y. Zhang, S. D. Chen, X. H. Niu, D. F. Xu, F. Chen, X. H. Chen, B. P. Xie, T. Zhang, and D. L. Feng, Sci. Rep. **4**, 5999 (2014).
[18] J. H. Han, A. Richardella, S. A. Siddiqui, J. Finley, N. Samarth, and L. Q. Liu, Phys. Rev. Lett. **119**, 077702 (2017).
[19] Y. Wang, D. P. Zhu, Y. Wu, Y. M. Yang, J. W. Yu, R. Ramaswamy, R. Mishra, S. Y. Shi, M. Elyasi, K. L. Teo, Y. H. Wu, and H. Yang, Nat. Commun. **8**, 1364 (2017).
[20] J. A. Sobota, S. Yang, J. G. Analytis, Y. L. Chen, I. R. Fisher, P. S. Kirchmann, and Z. X. Shen, Phys. Rev. Lett. **108**, 117403 (2012).
[21] Y. H. Wang, D. Hsieh, E. J. Sie, H. Steinberg, D. R. Gardner, Y. S. Lee, P. Jarillo-Herrero, and N. Gedik, Phys. Rev. Lett. **109**, 127401 (2012).
[22] S. Souma, K. Kosaka, T. Sato, M. Komatsu, A. Takayama, T. Takahashi, M. Kriener, K. Segawa, and Y. Ando, Phys. Rev. Lett. **106**, 216803 (2011).
[23] A. Crepaldi, B. Ressel, F. Cilento, M. Zacchigna, C. Grazioli, H. Berger, P. Bugnon, K. Kern, M. Grioni, and F. Parmigiani, Phys. Rev. B **86**, 205133 (2012).
[24] J. Sanchez-Barriga, E. Golias, A. Varykhalov, J. Braun, L. V. Yashina, R. Schumann, J. Minar, H. Ebert, O. Kornilov, and O. Rader, Phys. Rev. B **93**, 155426 (2016).
[25] K. Kuroda, J. Reimann, J. Gudde, and U. Hofer, Phys. Rev. Lett. **116**, 076801 (2016).
[26] K. Kuroda, J. Reimann, K. A. Kokh, O. E. Tereshchenko, A. Kimura, J. Gudde, and U. Hofer, Phys. Rev. B **95**, 081103(R) (2017).
[27] M. Hajlaoui, E. Papalazarou, J. Mauchain, G. Lantz, N. Moisan, D. Boschetto, Z. Jiang, I. Miotkowski, Y. P. Chen, A. Taleb-Ibrahimi, L. Perfetti, and M. Marsi, Nano Lett. **12**, 3532 (2012).
[28] M. Hajlaoui *et al.*, Nat. Commun. **5**, 3003 (2014).
[29] R. V. Aguilar, J. Qi, M. Brahlek, N. Bansal, A. Azad, J. Bowlan, S. Oh, A. J. Taylor, R. P. Prasankumar, and D. A. Yarotski, Appl. Phys. Lett. **106**, 011901 (2015).
[30] S. Sim, M. Brahlek, N. Koirala, S. Cha, S. Oh, and H. Choi, Phys. Rev. B **89**, 165137 (2014).
[31] S. Y. Maezawa, H. Watanabe, M. Takeda, K. Kuroda, T. Someya, I. Matsuda, and T. Suemoto, Sci. Rep. **5**, 16443 (2015).

[32] A. Q. Wu, X. Xu, and R. Venkatasubramanian, Appl. Phys. Lett. **92**, 011108 (2008).
[33] C. W. Luo, H. J. Wang, S. A. Ku, H. J. Chen, T. T. Yeh, J. Y. Lin, K. H. Wu, J. Y. Juang, B. L. Young, T. Kobayashi, C. M. Cheng, C. H. Chen, K. D. Tsuei, R. Sankar, F. C. Chou, K. A. Kokh, O. E. Tereshchenko, E. V. Chulkov, Y. M. Andreev, and G. D. Gu, Nano Lett. **13**, 5797 (2013).
[34] D. Hsieh, F. Mahmood, J. W. McIver, D. R. Gardner, Y. S. Lee, and N. Gedik, Phys. Rev. Lett. **107**, 077401 (2011).
[35] M. C. Wang, S. Qiao, Z. Jiang, S. N. Luo, and J. Qi, Phys. Rev. Lett. **116**, 036601 (2016).
[36] C. Kastl, C. Karnetzky, H. Karl, and A. W. Holleitner, Nat. Commun. **6**, 6617 (2015).
[37] Y. Xu, I. Miotkowski, C. Liu, J. F. Tian, H. Nam, N. Alidoust, J. N. Hu, C. K. Shih, M. Z. Hasan, and Y. P. Chen, Nat. Phys. **10**, 956 (2014).
[38] Z. Ren, A. A. Taskin, S. Sasaki, K. Segawa, and Y. Ando, Phys. Rev. B **82**, 241306(R) (2010).
[39] A. Akrap, M. Tran, A. Ubaldini, J. Teyssier, E. Giannini, D. van der Marel, P. Lerch, and C. C. Homes, Phys. Rev. B **86**, 235207 (2012).
[40] See Supplemental Material at http://link.aps.org/supplemental/10.1103/PhysRevLett.121.026807 for the carrier concentration calculation, which includes Ref. [41].
[41] N. W. Ashcroft and D. N. Mermin, *Solid State Physics* (Brooks-Cole, Belmont, MA, 1976).
[42] X. Liu and J. Sinova, Phys. Rev. Lett. **111**, 166801 (2013).
[43] H. Cao, C. Liu, J. Tian, and Y. Xu, arXiv:1409.3217.
[44] S. R. Park, W. S. Jung, C. Kim, D. J. Song, C. Kim, S. Kimura, K. D. Lee, and N. Hur, Phys. Rev. B **81**, 041405(R) (2010).
[45] Z. H. Zhu, G. Levy, B. Ludbrook, C. N. Veenstra, J. A. Rosen, R. Comin, D. Wong, P. Dosanjh, A. Ubaldini, P. Syers, N. P. Butch, J. Paglione, I. S. Elfimov, and A. Damascelli, Phys. Rev. Lett. **107**, 186405 (2011).
[46] C. T. Y. Chen, S. L. He, H. Weng, W. T. Zhang, L. Zhao, H. Y. Liu, X. W. Jia, D. X. Mou, S. Y. Liu, J. F. He, Y. Y. Peng, Y. Feng, Z. J. Xie, G. D. Liu, X. L. Dong, J. Zhang, X. Y. Wang, Q. J. Peng, Z. M. Wang, and S. J. Zhang, Proc. Natl. Acad. Sci. U.S.A. **109**, 3694 (2012).
[47] M. Bianchi, D. D. Guan, S. N. Bao, J. L. Mi, B. B. Iversen, P. D. C. King, and P. Hofmann, Nat. Commun. **1**, 128 (2010).
[48] Z. Luo, J. Tian, S. Huang, M. Srinivasan, J. Maassen, Y. P. Chen, and X. Xu, ACS Nano **12**, 1120 (2018).
[49] D. Hsieh, J. W. McIver, D. H. Torchinsky, D. R. Gardner, Y. S. Lee, and N. Gedik, Phys. Rev. Lett. **106**, 057401 (2011).
[50] D. Hsieh, Y. Xia, D. Qian, L. Wray, J. H. Dil, F. Meier, J. Osterwalder, L. Patthey, J. G. Checkelsky, N. P. Ong, A. V. Fedorov, H. Lin, A. Bansil, D. Grauer, Y. S. Hor, R. J. Cava, and M. Z. Hasan, Nature (London) **460**, 1101 (2009).
[51] L. Fu, Phys. Rev. Lett. **103**, 266801 (2009).
[52] M. S. Bahramy, P. D. C. King, A. de la Torre, J. Chang, M. Shi, L. Patthey, G. Balakrishnan, P. Hofmann, R. Arita, N. Nagaosa, and F. Baumberger, Nat. Commun. **3**, 1159 (2012).
[53] W. Jung, Y. Kim, B. Kim, Y. Koh, C. Kim, M. Matsunami, S. I. Kimura, M. Arita, K. Shimada, J. H. Han, J. Kim, B. Cho, and C. Kim, Phys. Rev. B **84**, 245435 (2011).
[54] Y. H. Wang, D. Hsieh, D. Pilon, L. Fu, D. R. Gardner, Y. S. Lee, and N. Gedik, Phys. Rev. Lett. **107**, 207602 (2011).
[55] S. Winnerl, M. Orlita, P. Plochocka, P. Kossacki, M. Potemski, T. Winzer, E. Malic, A. Knorr, M. Sprinkle, C. Berger, W. A. de Heer, H. Schneider, and M. Helm, Phys. Rev. Lett. **107**, 237401 (2011).
[56] V. Iyer, P. Ye, and X. Xu, 2D Mater. **4**, 021032 (2017).
[57] F. X. Xiu, L. A. He, Y. Wang, L. N. Cheng, L. T. Chang, M. R. Lang, G. A. Huang, X. F. Kou, Y. Zhou, X. W. Jiang, Z. G. Chen, J. Zou, A. Shailos, and K. L. Wang, Nat. Nanotechnol. **6**, 216 (2011).
[58] M. Konig, M. Baenninger, A. G. F. Garcia, N. Harjee, B. L. Pruitt, C. Ames, P. Leubner, C. Brune, H. Buhmann, L. W. Molenkamp, and D. Goldhaber-Gordon, Phys. Rev. X **3**, 021003 (2013).
[59] J. Dufouleur, L. Veyrat, B. Dassonneville, C. Nowka, S. Hampel, P. Leksin, B. Eichler, O. G. Schmidt, B. Buchner, and R. Giraud, Nano Lett. **16**, 6733 (2016).
[60] J. Bass and W. P. Pratt, J. Phys. Condens. Matter **19**, 183201 (2007).
[61] J. Sanchez-Barriga, M. Battiato, E. Golias, A. Varykhalov, L. V. Yashina, O. Kornilov, and O. Rader, Appl. Phys. Lett. **110**, 141605 (2017).
[62] M. Neupane, S. Y. Xu, Y. Ishida, S. Jia, B. M. Fregoso, C. Liu, I. Belopolski, G. Bian, N. Alidoust, T. Durakiewicz, V. Galitski, S. Shin, R. J. Cava, and M. Z. Hasan, Phys. Rev. Lett. **115**, 116801 (2015).
[63] C. Mai, A. Barrette, Y. F. Yu, Y. G. Semenov, K. W. Kim, L. Y. Cao, and K. Gundogdu, Nano Lett. **14**, 202 (2014).
[64] F. Mahmood, Z. Alpichshev, Y. H. Lee, J. Kong, and N. Gedik, Nano Lett. **18**, 223 (2018).
[65] R. Schmidt, G. Berghauser, R. Schneider, M. Selig, P. Tonndorf, E. Malic, A. Knorr, S. M. de Vasconcellos, and R. Bratschitsch, Nano Lett. **16**, 2945 (2016).